Behaviour of small regions of different gases carried in accelerated gas flows

By GEORGE RUDINGER AND LOWELL M. SOMERS
Cornell Aeronautical Laboratory, Buffalo, New York

(Received 2 April 1959)

Small regions in a flow where the density is different from that of the surrounding gas do not exactly follow accelerated motions of the latter, but move faster or slower depending on whether their density is smaller or larger than that of the main flow. This behaviour cannot be quantitatively explained by treating a gas 'bubble' as a hypothetical solid particle of the same density, because a gas bubble cannot move relative to the surrounding gas without being transformed into a vortex which absorbs part of the energy of the relative motion.

To illustrate the acceleration effect, the flow velocity behind known pressure waves in a shock tube is compared with the observed velocity of a bubble produced by a spark discharge. The displacement of such a bubble by a wave exceeds that of a flow element by more than 20 %, but the bubble density is not known. If the spark discharge is replaced by a small jet of another gas, a pressure wave cuts off a section of this jet which then represents a bubble of known density.

A theory is developed which permits computing the response of such bubbles to accelerations. The ratio of the bubble velocity to the velocity of the surrounding gas depends on the density ratio for the two gases and on the shape of the bubble, but not on the acceleration. Experimental results with H_2, He, and SF_6 bubbles in air, accelerated by shock waves of various strength, are presented and agree well with the theoretical predictions. The results apply regardless of whether accelerations are produced by pressure waves in a non-steady flow or by curvature of streamlines in a steady flow. Various aspects of the experimental observations are discussed.

1. Introduction

The technique of using tracers for the visualization of streamlines in a gas flow, or for the measurement of flow velocity, is well established. It is also known that such tracers do not move exactly with the flow if their density is different from that of the surrounding gas and if they have to undergo accelerated motions. The behaviour of solid particles under such conditions was described in considerable detail, for instance, by Wright (1951), Cady (1954), and Hoenig (1957). While such particles always lag in accelerated flows, gaseous particles ('bubbles') may lead or lag depending on whether their density is smaller or larger than that of the surrounding gas. The behaviour of gas bubbles in accelerated flows is, however, different from that of a hypothetical solid particle of the same density, because a gas bubble cannot move relative to the surrounding gas without being trans-

formed into a vortex which absorbs part of the energy of the relative motion. This effect appears to have received little attention, although its understanding is important not only when gas bubbles are used as tracers but also for other phenomena. For example, if pressure waves interact with a flame, the different responses of the regions of different density lead to a deformation of the flame front; this modifies the rate of heat release, and causes secondary waves to be emitted by the flame. Such waves were observed, for instance, by Markstein (1957), and the theoretical and experimental aspects of such interactions were reviewed by Rudinger (1958).

Gaseous tracer bubbles can be produced by various methods, and such techniques, developed mainly for the measurement of constant flow velocities, were reviewed by Cady (1954). A method to measure not only velocities but also velocity distributions is due to Townend (1937), who discharged straight sparks between two electrodes and determined the subsequent motion and deformation of the spark columns. A spark column, consisting of hot gas, can be observed by means of a schlieren system. In an alternative method, a number of sparks, discharged in rapid succession, can be photographed directly. In the latter method, each spark tends to follow the ionized path of the preceding one, and, since the spark columns are carried with the flow, their displacements and deformations indicate the local flow velocity. This multiple-spark technique has also been studied by Saheki (1947), and by Bomelburg (1956), Herzog (1957), Herzog & Weske (1957), and Weske (1958). The errors made by neglecting the response of the spark column in accelerated flows are not negligible, and Herzog & Weske (1957) propose a semi-empirical method of correction.

In §§ 2 and 3, shock-tube experiments are described in which the flow velocities, produced by pressure waves of known properties, are compared with the velocities of spark-heated bubbles to illustrate the large errors that may result if such bubbles are used as tracers in a flow. Since the effective density of a spark-column is not known, a new technique for producing bubbles of known density is described in § 4, and a theory of wave interaction with such bubbles is derived in § 5. The theoretical and experimental results are compared and discussed in § 6.

2. Apparatus for spark experiments

The response of gas bubbles to accelerations is conveniently studied by means of a shock tube. In the first experiments, bubbles are produced by an electric spark discharge, and their motion is observed with the aid of a schlieren system.

A vertical shock tube is used for these experiments. It has a square cross-section of 3 in. width and a total length of about 9 ft. The diaphragm is located 3 ft. from the top, and the last 9 in. from the bottom represent the test section which is provided with two glass walls for the schlieren observations. To produce shock or expansion waves of desired strength, the initial pressure in the test section is always atmospheric and the pressure in the driver section is raised or lowered as needed. One or more layers of photographic film are used as diaphragms and are punctured by a solenoid-operated plunger needle. Details of the construction of the shock tube have been published elsewhere (Markstein 1957).

A spark gap is formed between one wall of the test section and the point of a steel needle, introduced through the opposite wall. The spark is produced by charging a 1μF condenser to 400 V and then discharging it through an automobile spark coil in series with a 3 D 22 thyratron. The latter acts as a switch for proper timing control. In agreement with observations by previous investigators (Townend 1937, Saheki 1947 and Bomelburg 1956), reproducible straight sparks can be obtained if the needle electrode is negative and if the gap does not exceed about $\frac{3}{8}$ in. To assure that the spark is discharged at right angles to the shock-tube wall, the latter is covered with an insulating sheet (photographic film) with a pin hole opposite the needle. The spark-heated column of air is clearly visible on schlieren photographs obtained with a short-duration spark light source.

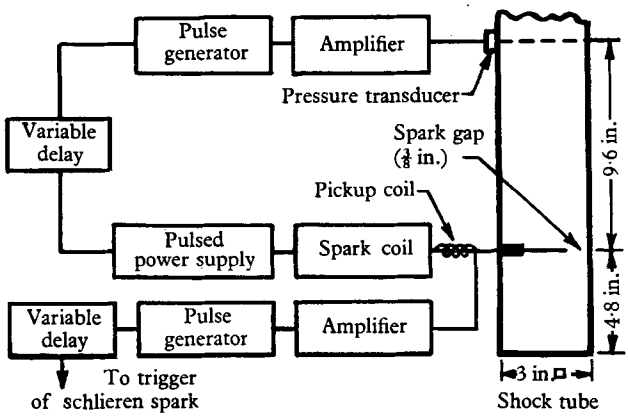

FIGURE 1. Schematic arrangement of shock tube and instrumentation for spark experiments.

The experimental set-up is shown schematically in figure 1. Proper timing of the spark discharge and of the schlieren spark is achieved by means of two variable-time delays. A pressure transducer is mounted near the top of the test section, so that the amplified signal from a pressure wave propagating down the tube triggers a thyratron several hundred microseconds before the wave reaches the spark gap. The thyratron circuit produces a single pulse which, in turn, triggers the spark discharge after a desired delay. A pick-up coil, consisting of a few turns of wire wrapped around the high-tension lead of the spark, produces a signal which, through a second thyratron pulse generator and the second delay unit, triggers the schlieren spark.

3. Measurements of flow velocity behind pressure waves

In the first series of experiments, the displacement of the spark column in the wake of a weak shock wave is measured as a function of time and compared with the corresponding displacement of an element in the surrounding gas. The spark is discharged shortly before the arrival of the wave at the spark gap, and a schlieren photograph is taken after some interval. Figure 2*a*, plate 1, shows a typical record.

Such photographs can be evaluated with reference to the wave diagram in figure 3*a* which shows the motion of the shock wave, the spark column, and

a corresponding gas element. Let x_S be the distance of the shock wave from the spark gap at the time the schlieren photograph is taken. If this distance is plotted as a function of the delay setting for the schlieren spark, one obtains a straight line which intercepts the line $x_S = 0$ at the instant that the shock wave passes the spark gap. Let Δt be the time interval in which the wave has travelled the distance x_S. These data determine the shock velocity and, together with the initial speed of sound in the test section a_0, the shock Mach number M_S. For the weak shocks used in these experiments, the results agree well with calculated data based on the theory of an ideal shock tube.

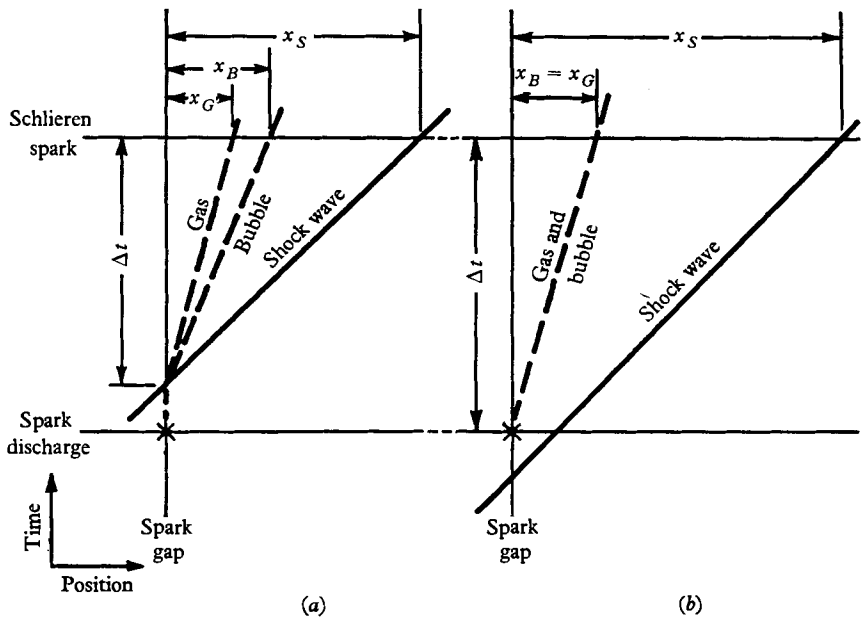

FIGURE 3. Wave diagrams for spark experiments with the spark discharged: (*a*) before, and (*b*) after, passage of a shock wave.

The spark bubble remains at rest until the shock wave arrives; it then travels the distance x_B during the time Δt. During the same time, a gas element that initially was located at the spark gap travels the distance x_G. If the flow were accurately represented by the bubble motion, the ratio of the two displacements should be unity. Since $\Delta t = x_G/u_G = x_S/(a_0 M_S)$, where u_G is the flow velocity of the gas, the actual displacement ratio is given by

$$\frac{x_B}{x_G} = \frac{x_B}{x_S}\frac{a_0 M_S}{u_G}. \tag{1}$$

The first factor on the right-hand side of this equation can be obtained directly from the schlieren photographs, and the second factor varies only with M_S, since u_G is related to M_S and a_0 by

$$u_G = \frac{2}{\gamma+1} a_0 \left(M_S - \frac{1}{M_S}\right), \tag{2}$$

where γ is the ratio of the specific heats. The displacement ratios observed for shock Mach numbers of about 1·12, 1·22 and 1·28, corresponding to shock-pressure ratios of 1·29, 1·58 and 1·74, respectively, are plotted in figure 4. This plot indicates that the velocity of a spark-heated bubble immediately after interaction with a shock wave is about 60 % higher than the flow velocity. Subsequently, the bubble velocity decreases and gradually approaches the flow velocity. In spite of the scatter of the data, the uncertainty of the measured bubble displacements is considerably smaller than the deviation of the displacement ratio from unity, as can be seen in figure 2*a*, plate 1, where the value of x_G is also indicated.

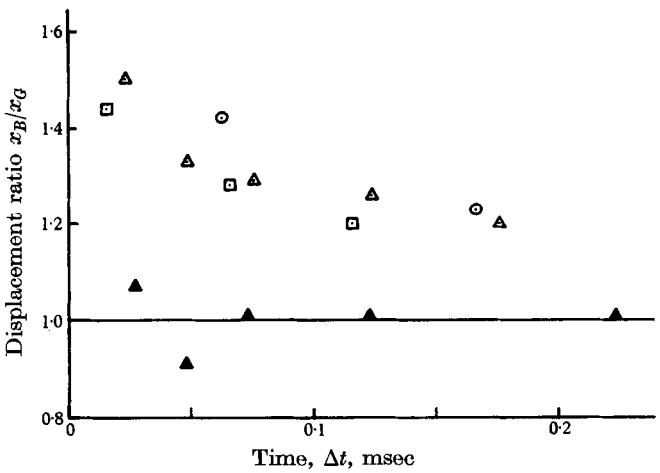

FIGURE 4. Displacement ratios of spark bubbles for shock waves of various strength as a function of the travel time of the bubbles. Spark is discharged either before (open symbols) or after (filled symbols) passage of the shock wave. Shock pressure ratio: ⊙, 1·29; △, ▲, 1·58; ⊡, 1·74.

To verify that the observed deviations of the displacement ratio from unity are caused by the interaction of the shock wave with the spark volume, the bubble displacement is also determined in experiments in which the spark is discharged after the shock wave has passed the spark gap. A typical schlieren photograph is shown in figure 2*b*, plate 1, and the wave diagram corresponding to these experiments is given in figure 3*b*. The travel time of the bubble Δt is determined by the setting of the second delay unit (see figure 1), but a correction must be applied because of unavoidable fixed delays in the spark circuits. This correction is obtained by plotting x_B as a function of the delay setting and extrapolating to $x_B = 0$. The displacement ratio x_B/x_G is then obtained from the measured value of x_B and from $x_G = u_G \Delta t$. The results are indicated in figure 4 by the filled-in symbols and verify that the bubble moves with the flow as long as accelerations are absent.

From the data presented in figure 4, it appears that the excess bubble velocity depends only little, if at all, on the strength of the shock wave. Although the shock accelerations are extremely high, the shock Mach number is varied over a small range only. The effect of accelerations of a different order of magnitude can be studied by experiments in which the spark column is accelerated by an

expansion wave. Such waves are produced by partially evacuating the driver section of the shock tube, and their properties can be determined from oscilloscope records of the pressure variations at the location of the pressure transducer (see figure 1). The expansion wave is reflected from the closed end of the shock tube and leaves a region of reduced density and zero velocity. If the spark is discharged before arrival of the wave and the schlieren photograph taken after passage of the reflected wave, the bubble displacement x_B is readily compared with the corresponding displacement of a gas element x_G. To test for proper timing of the events, the starting pulse from the second time-delay (see figure 1) is also used to produce a signal on a second channel of the oscilloscope to mark the instant of the spark discharge. The instant of the schlieren spark is similarly indicated on the pressure record. Figure 5, plate 1, shows a schlieren photograph with the corresponding oscilloscope record, where it can be seen that the spark is discharged before the pressure starts to decrease, and that the photograph is taken after the pressure again has become steady. The interval between the spark discharge and the taking of the photograph is about 4·5 msec. A spark column of this 'age' no longer appears as a straight line but as a bubble of irregular shape. The mean of the maximum and minimum distances of the bubble boundaries from the spark gap is, therefore, taken as x_B.

During the passage of the incident and reflected expansion waves, the density decreases from ρ_0 to ρ_∞, and this change can be computed from the corresponding pressure change since the flow is isentropic. Let L be the distance of the spark gap from the closed end of the shock tube. The value of x_G is then related to the densities and pressures by

$$\frac{x_G+L}{L} = \frac{\rho_0}{\rho_\infty} = \left(\frac{p_0}{p_\infty}\right)^{1/\gamma}. \tag{3}$$

The pressure ratio p_∞/p_0 for these experiments is in the neighbourhood of 0·7. For the record in figure 5, plate 1, $p_\infty/p_0 = 0{\cdot}66$, and the value of x_G computed from equation (3) is indicated in the figure. Because of the uncertainty of x_B, the displacement ratios scatter considerably, and the observed values range from about 1·15 to 1·25. Since gradual cooling of the bubble during its acceleration and deceleration by the waves tends to reduce the excess displacement, these values seem sufficiently close to those observed for shock accelerations (figure 4) to support the previous conjecture that the displacement ratio is independent of the applied acceleration.

4. Experiments with bubbles of known density

The experiments described above give a good indication of how pressure waves interact with bubbles the density of which is different from that of the surrounding gas, but the experimental results cannot be used to check a theoretical analysis because the density of a spark-heated bubble is not known. A technique was developed, therefore, to produce bubbles of known density.

At first, soap bubbles filled with various gases were tried, but this approach was soon abandoned. The displacement of large bubbles amounts to only a few bubble diameters and cannot be measured accurately because of changes of bubble shape.

For small bubbles, the mass of the soap film represents a significant fraction of the total mass, so that the bubble density becomes uncertain.

In the technique finally adopted, a fine jet of some gas, discharged across the shock tube, represents a 'bubble' of known density. For this purpose, the needle electrode of the spark gap is replaced by a piece of hypodermic tubing of 0·033 in. internal diameter. A second tube of about 0·25 in. diameter is mounted in the opposite wall of the test section to receive the jet discharged by the fine tube. The larger tube is connected to an aspirator pump to remove the jet flow before it can contaminate the air in the test section. The gap between the two tubes is about 0·3 in. so that a passing shock wave cuts off this exposed length of the jet. The motion of this jet element can then be observed with the aid of a schlieren system.

Figure 6, plate 2, shows four schlieren photographs obtained by this technique for a shock-pressure ratio of about 1·3. The gases used are hydrogen, helium, and sulphurhexafluoride. Such records can be evaluated by the procedure already described in connexion with the spark experiments, and the values of x_G corresponding to the experimental conditions are marked in the figure. It is seen that the displacements of the bubbles are larger than x_G for the light gases H_2 and He, and smaller for the heavy gas SF_6.

One interesting feature of these photographs is that all bubbles are inclined although the jet is discharged horizontally. This phenomenon is readily explained. The pure gas that leaves the jet tube mixes with air as it advances across the test section. Consequently, the effective density of the bubble changes continuously from that of the pure gas to that of a mixture of this gas with air. The bubble end nearest the jet tube, therefore, travels faster than the other end for H_2 and He, and slower for SF_6. Because of the rapid deterioration of the SF_6 bubble, which is discussed in § 6, the inclination of this bubble is clearly visible only on photographs taken early enough after passage of the shock wave (lower right picture of figure 6, plate 2).

The extent to which the jet mixes with air, and therefore the inclination of the bubble, depends on the diffusion rate and on the jet velocity which controls the time available for mixing. No attempt was made to keep the jet velocity the same for all gases, and the photographs indicate that the velocity of the H_2 jet was considerably higher than that of the He jet, because the He bubble is more inclined than the H_2 bubble in spite of the 10 % larger diffusion coefficient for H_2-air as compared to He-air (Hirschfelder, Curtis & Bird 1954).

In view of the foregoing discussion, all bubble displacements must be measured on the side of the bubble nearest to the jet tube. Experimental results obtained with the described technique are discussed in § 6.

5. Theory of wave interaction with gas bubbles

For an observer moving with the gas, the acceleration by a wave is equivalent to that of a gravitational field. In this field, two forces act on a bubble in the gas, namely, its weight in the equivalent gravitational field and a buoyancy force equal to the corresponding weight of the gas displaced by the bubble. Those two forces act in opposite directions and are of equal magnitude only if the density of the bubble is the same as that of the surrounding gas. If the bubble moves because the

resultant force is not zero, its surface becomes a sheet of vorticity. Subsequently, this sheet rolls up with the result that the entire bubble is transformed into a vortex. The effect of this transformation corresponds to a drag on the translational bubble motion relative to the gas which must supply the energy absorbed by the vortex flow.

Vortex formation is not readily apparent in the described experiments because the bubbles are too small to reveal sufficient details of the flow, although figures 2*a* and *b*, plate 1, indicate the more 'turbulent' character of a bubble that has undergone interaction with a shock wave as compared to the smooth surface of a bubble that has not interacted. The development of a vortex can be clearly seen in figure 7, plate 3, which shows three stages of the interaction of a shock wave with a flame bubble. These schlieren photographs are taken from a series obtained by Markstein (1958) in the course of another investigation. A combustible mixture in the test section of the shock tube is ignited by a spark between the electrodes, visible at the centre of each photograph, and a bubble of burned gas is contained within the flame front. The latter advances so slowly that its progress during the time of interest here is unimportant. The first photograph shows the approximate spherical flame bubble just before interaction with a downward-travelling shock wave. The second photograph shows the wave emerging from the bubble and also a reflected wave. In the third photograph, the waves have moved away from the bubble which has now, clearly, been transformed into a vortex ring.

The following analysis by-passes a detailed study of this vortex formation and yields the final translational velocity of the bubble directly on the basis of a few plausible assumptions. Consider, first, accelerations by shock waves. The time during which a shock wave passes through the bubble, i.e. the time during which acceleration takes place, is so short that the vortex must essentially be formed in a second, subsequent stage. This view is supported by figure 7, plate 3, where no indication of vortex formation can be seen at the time when the shock wave has left the bubble. The analysis will, therefore, proceed in two steps, corresponding to the initial acceleration of the bubble and to its subsequent transformation into a vortex. Later, it will be shown that, within the accuracy of the assumptions made, the same two-step analysis may also be applied to waves, other than shock waves, for which acceleration and vortex formation take place simultaneously.

During the acceleration stage, the bubble distortion may be ignored (centre of figure 7, plate 3), and it seems permissible to treat the initial phase of the motion in the following way. Let the subscript P identify the quantities associated with the bubble motion immediately following the passage of the shock, and let the subscript G identify the quantities associated with the ambient gas particles. Assuming that one may neglect the modification of the pressure field caused by the presence of the bubble, the impulse per unit volume I which the bubble experiences during the shock passage is precisely that which the ambient gas would have experienced, namely, $I = \rho_G u_G$, where u_G is the gas velocity after the shock has passed.

This impulse must accelerate the bubble from rest to the speed u_P and must also accelerate some of the surrounding gas from the speed u_G to a velocity distribution associated with the motion of the bubble. Since the latter is not

distorted during this early phase, the bubble may be treated as if it were a solid particle. One may thus invoke the well-known concept of 'apparent additional mass' (virtual mass) for such a situation and obtain

$$I = \rho_G u_G = \rho_P u_P + k\rho_G(u_P - u_G), \tag{4}$$

with k as the apparent additional mass fraction (i.e. inertia coefficient). For a spherical bubble, $k = 0{\cdot}5$, and for a long circular cylinder moving at right angles to its axis, $k = 1{\cdot}0$ (Lamb 1945, p. 155). Equation (4) yields directly

$$u_P = \frac{1+k}{\sigma+k} u_G, \tag{5}$$

where

$$\sigma = \frac{\rho_P}{\rho_G} = \frac{\rho_B}{\rho_G} \tag{6}$$

is the density ratio. For real solid particles, such as are customarily used for flow visualization, σ is of the order of 1000, so that u_P is practically zero. For σ less than unity, the particle velocity exceeds that of the gas. The foregoing part of the analysis is closely related to calculations described by Birkhoff & Caywood (1949) who considered accelerated motions of gas bubbles in a liquid.

The second step of the analysis deals with the transformation of a gas bubble into a vortex as a result of the initial motion relative to the surrounding gas. Since the kinetic energy of the initial motion must supply the energy absorbed by the vortex, the relative velocity is reduced from $u_P - u_G$ to $u_B - u_G$, where u_B is the desired final bubble velocity. Let the ratio of these relative velocities be denoted by β, so that

$$u_B - u_G = \beta(u_P - u_G). \tag{7}$$

The quantity β^2 thus represents the fraction of the kinetic energy of the initial relative bubble motion that is available for the final relative translational motion. Substitution of equation (5) into equation (7) yields the final bubble velocity relative to the duct as

$$u_B = \left(1 + \beta\frac{1-\sigma}{\sigma+k}\right) u_G, \tag{8}$$

where β is yet to be determined.

Figure 7, plate 3, indicates that a spherical bubble is transformed into a vortex ring, and it seems plausible that an infinitely long cylindrical bubble would become a linear vortex pair. These two cases can be treated theoretically, and the bubble motions observed in the described experiments should then fall between those corresponding to these extremes.

The calculations for a vortex ring are based on a study by Taylor (1953). He considers a flat circular disk that is suddenly set in motion along the axis of symmetry, in a perfect fluid, and without separation of the flow. If the material of the disk were then suddenly 'dissolved away', the flow could also be considered as being caused by a distribution of vortex lines over the plane of the disk. The strongest vortex lines near the edge of the disk tend to roll up the weaker ones until, finally, a vortex ring remains for which it is assumed that the vorticity is uniformly distributed over a core of small diameter compared to the diameter of the ring. Such a vortex cannot remain at rest in the surrounding gas, but moves with a velocity that depends on its dimensions and strength. To apply Taylor's

results to the present problem, the assumption is made that this vortex ring represents a reasonable approximation of the vortex into which a spherical gas bubble is transformed, provided the initial velocity of the bubble is equal to that of the disk. Taylor derives the ratio of the velocity of the vortex relative to the fluid to the initial velocity of the disk. This ratio has been defined here as β, and Taylor's results is $\beta = 0{\cdot}436$.

If the circular disk in Taylor's analysis is replaced by an infinite lamina, a linear vortex pair is formed which, by analogy with the preceding case, is considered to be an approximation to the vortex into which a cylindrical bubble is transformed. This analysis is presented in the Appendix and yields $\beta = 0{\cdot}203$.

The foregoing treatment gives no indication of the time required for the vortex to form, but figure 7, plate 3, shows that the vortex is fully developed before the bubble has travelled one bubble diameter. Since the displacements of interest have a magnitude of many such diameters (see figure 6, plate 2), it may be assumed that the vortex motion is instantaneously established. As a consequence of this assumption, equation (8) may be applied also to waves other than shock waves. Such waves can always be approximated as closely as desired by a sequence of discontinuous wave elements for each of which the ratio of the velocity increments $\Delta u_B/\Delta u_G$ has the same value. If the two steps of the analysis were applied to each element consecutively, the final result would thus be the same as if the analysis had been applied to the entire wave, provided only that the bubble density is not significantly changed by diffusion during the time of wave interaction with the bubble.

Two possible sources of error in the analysis should be discussed. Buoyancy of a bubble in the gravitational field of the earth causes a bubble motion that is superposed on the motion produced by a wave. Although the acceleration of this motion is several orders of magnitude smaller than the wave acceleration, it acts during the entire experiment while the wave acts only during its passage across the bubble. For the conditions of the present experiments, it is readily verified that this effect is utterly negligible if the travel time of the bubble is less than 1 msec, and even for travel times of 5 msec, as in the experiments with the expansion waves (figure 5, plate 1), the displacement caused by gravity alone is less than 3 % of the total bubble displacement.

The other effect to be considered is related to differences in compressibility of the two gases involved. In the derivation of equation (8), it has been implied that the density ratio remains constant during the acceleration of the bubble. This condition is satisfied only if the gases have the same compressibility. If the compressibilities are not equal, the density ratio changes during passage of the wave from σ_0 to σ_∞, which is given by

$$\sigma_\infty = \sigma_0 \left(\frac{p_\infty}{p_0}\right)^{(1/\gamma_B)-(1/\gamma_G)}, \tag{9}$$

where p_∞/p_0 is the pressure ratio across the wave. The relation for isentropic changes of state may be used because only weak waves are considered here. Since an effective value of the density ratio must lie between σ_0 and σ_∞, the influence of this uncertainty of σ on u_B in equation (8) is less than 0·5 % for the conditions of

the reported experiments ($p_\infty/p_0 < 2$, $\gamma_G = 1{\cdot}40$ for air, $\gamma_B = 1{\cdot}10$ for SF_6, and $\gamma_B = 1{\cdot}67$ for He).

In the described experiments, the ratio of bubble length to its diameter is about 9. If this shape is considered as an elongated ellipsoid of revolution, the inertia coefficient (Lamb 1945, p. 155) is approximately 0·94. In view of the uncertainty of the effective shape of the bubbles, the value $k = 1{\cdot}0$, corresponding to an infinite cylinder, is used. The effect on u_B of such a variation of k in equation (8) is unimportant.

			u_B/u_G	
Gas	σ	u_P/u_G	Vortex ring	Vortex pair
H_2	0·0695	1·87	1·38	1·18
He	0·138	1·76	1·33	1·15
SF_6	5·03	0·33	0·71	0·86

TABLE 1. Theoretical results

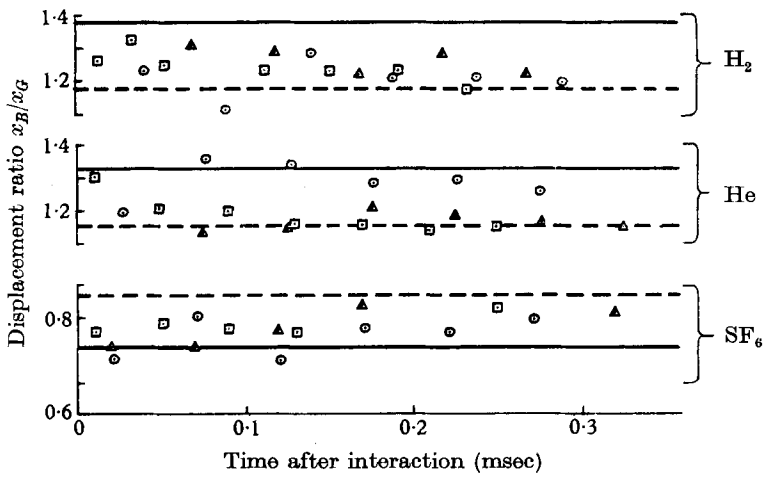

FIGURE 8. Observed and theoretical displacement ratios for the interaction of shock waves with gas bubbles of different densities (see also Table 1). ——, Vortex ring; – – –, vortex pair. Shock pressure ratio: ⊙, 1·29; △, 1·58; □, 1·74.

Experimental results should lie between the values predicted by equation (8) for the two values of β, corresponding to a vortex ring and a linear vortex pair, respectively. For the gases used, the initial and final velocity ratios, u_P/u_G and u_B/u_G, as computed from equations (5) and (8), are collected in table 1.

Figure 8 shows the theoretical and experimental displacement ratios plotted as a function of the time elapsed after interaction of the shock wave with the bubble. The pressure ratios of the shock waves used in the experiments are 1·29, 1·58 and 1·74, and the experimental points are identified accordingly. The theoretical values are independent of time and are thus represented by horizontal lines.

6. Discussion

The effect of accelerations in a gas flow on the motion of gas bubbles of different density has been studied both theoretically and experimentally. In the present investigation only one-dimensional flows accelerated by pressure wave are considered, but it should be emphasized that it is irrelevant whether the accelerations occur in a non-steady flow or are caused by curvature of streamlines in a steady flow. The behaviour of gas bubbles in an accelerated flow is quite different from that of solid particles and cannot be explained by the difference in density alone. If a shock wave passes over a solid particle, which may be about 1000 times as dense as the surrounding gas, the initial particle velocity is practically zero. Subsequently, the particle speeds up under the influence of its aerodynamic drag until it moves with the flow. A gas bubble, on the other hand, acquires almost instantaneously, a velocity that may be larger or smaller than the gas velocity, depending on whether the density ratio is smaller or larger than unity. This velocity is, however, different from that of a hypothetical solid particle of the same density because a gas bubble in relative motion with respect to its surroundings is transformed into a vortex which absorbs part of the energy. Subsequently, the relative bubble velocity gradually decreases as a result of viscous dissipation.

The theory is based on the assumption that a spherical bubble is transformed into a vortex ring, and a cylindrical bubble into a linear vortex pair. One obtains for these limiting cases bubble velocities that differ by less than 20 % for the gases used here, and the velocities for other bubble shapes should fall between these rather narrow limits. The experimental data in figure 8 are in good agreement with this requirement and thus support the main features of the theory, namely, that the vortex is formed practically instantaneously (before the bubble has travelled one bubble diameter), and that the velocity and displacement ratios are independent of the magnitude of the acceleration.

According to equation (7), β^2 represents the fraction of the energy of the initial relative bubble motion that is available for translational motion after a vortex is formed. The effective value of β should lie between 0·203 and 0·436, so that the major fraction of the energy is absorbed by the vortex, and only about 10 % remain for the translational motion.

It is interesting to compare the results for gas bubbles with those for solid tracer particles, for example, those given by Hoenig (1957). A shock wave of Mach number 10, propagating in argon of 273 °K, at a pressure of 1 cm of mercury, produces a flow velocity of $2{\cdot}42 \times 10^5$ cm/sec. A particle of 10^{-3} cm diameter and a density of 3 g/cm^3 remains practically at rest immediately after passage of the shock wave, and reaches 95 % of the gas velocity after about 0·15 msec. After this time, the particle follows the flow closely. By comparison, the decrease of the relative velocity of a gas bubble behind a shock wave is so slow that it is barely noticeable in figure 8. The displacement ratios for H_2 and He show a tendency to decrease and those of SF_6 to increase with time, but the decay of the relative motion is still smaller than the scatter of the experimental points even after 0·3 msec.

The displacement of a gas bubble that initially is moving with the flow can always be considered as the vector sum of two displacements, one that would be observed if the flow velocity remained constant, and the other caused by accelerations. The former exactly represents the corresponding motion of the flow, while the latter differs from that of the flow by the factor $1+\beta(1-\sigma)/(\sigma+k)$, according to equation (8). This factor is independent of the manner in which the acceleration takes place as long as σ may be treated as a constant. If the acceleration lasts long enough for σ to change significantly as a result of diffusion and/or heat conduction, the foregoing constant factor no longer applies. Dissipation of vorticity because of viscosity also reduces the relative bubble motion. The effect of diffusion, which causes the sloping appearance of the bubbles in figure 6 (plate 2), has been discussed in § 4. Although one is dealing there with variations of σ in space rather than in time, these effects are closely related.

Another interesting feature of the behaviour of gas bubbles is the instability of bubbles that are heavier than their surroundings. Figure 6, plate 2, illustrates the rapid disintegration of SF_6 bubbles, while H_2 and He bubbles maintain their appearance for considerably longer times. Similar observations about the stability of buoyant vortices were reported by Turner (1957), who also provided the explanation that a light vortex core stabilizes the motion in a manner comparable to that of a stable stratification of two gases in a gravitational field, except that, in the vortex, gravity is replaced by the centrifugal force due to rotation.

Figure 4 shows that the displacement ratio of spark-heated bubbles decreases rather rapidly, while figure 8 indicates almost constant values for bubbles of the three gases used. The main difference between these experiments is that spark-heated bubbles are much hotter than the surrounding gas, while the temperature of the gas bubbles differs only a little if at all. It is readily verified that the compression produced by the strongest shock waves used in the experiments causes differences between bubble and gas temperatures of 0 °K for H_2, 23 °K for He, and -23 °K for SF_6 if the initial air temperature is 300 °K. Heat conduction and viscosity effects should, therefore, become significant mainly for the spark-heated bubbles. The consequences of these effects are not included in the theory, and only a tentative explanation of the observed behaviour is offered here. It should first be noted that, although the density of a spark-heated bubble is not known, the value of the displacement ratio computed from equation (8) cannot exceed $1+\beta$, corresponding to $\sigma = 0$, and for $k = 1{\cdot}0$. Extrapolation of the experimental data in figure 4 to the origin of the time scale should, therefore, yield a value between about 1·2 and 1·4, depending on the effective value of β, but the experimental data indicate an initial displacement ratio in the neighbourhood of 1·6. The observed results for small values of Δt seem, therefore, too high to represent the decay of a vortex. The data lie between the values corresponding to a fully developed vortex, as given by equation (8) and those corresponding to the initial bubble velocity before a vortex is formed, as given by equation (5), but there seems to be no reason why the transformation of a hot bubble into a vortex should be slower than that of a cold bubble. The high bubble velocities may be explained by considering the effect of cooling on the vortex. The propagation velocity of a vortex relative to the surrounding gas is proportional to the circula-

tion and inversely proportional to the size of the vortex (see, for example, equation (A 5) of the Appendix). While cooling does not affect the circulation, it causes the vortex to contract and, therefore, to speed up. According to this hypothesis, the behaviour of spark-heated bubbles, as shown in figure 4, is an indication of the extent to which the slowing down of the bubble because of vortex formation is counteracted by a speeding up due to cooling.

The large viscosity of air at elevated temperatures should cause a rapid dissipation of vorticity. An analysis of the slope of the relation between the displacement ratio and time (figure 4) shows indeed that after about 0·2 msec, the bubble velocity is already reduced to within a few per cent. of the flow velocity. It appears therefore that, immediately after interaction, the behaviour of a spark-heated bubble is significantly affected by cooling, while later, the viscosity effects dominate.

If spark-heated bubbles are used for tagging a flow, a correction for acceleration effects may have to be made to avoid appreciable errors, particularly immediately after accelerations. For bubbles formed by different gases, the acceleration effects can be greatly reduced by selecting density ratios as close to unity as the sensitivity of the detection system permits. In the described experiments, rather extreme conditions are used to demonstrate the phenomena clearly and to provide a sensitive test for the theory. The described results not only have a direct bearing on the use of tracer bubbles in gas flows, but they may also contribute to the understanding of various phenomena in flows of non-uniform density.

The authors wish to thank their colleagues G. H. Markstein and A. Gail for stimulating discussions in the course of this work. This work was started as an internal research project of Cornell Aeronautical Laboratory, and continued under the auspices of Project SQUID which is supported by the Office of Naval Research under Contract *Nonr*-1825(25).

Appendix

Impulsive motion of an infinite lamina and subsequent formation of a linear vortex pair

Taylor (1953) analysed the formation of a ring vortex under the condition that an impulse is given to a circular disk and the latter is then 'dissolved away' A similar analysis is carried out in the following for an infinite lamina.

Assume that a lamina of width $2b$ is suddenly moved with a velocity U at right angles to its plane and that no flow separation occurs. A discussion of the resulting potential flow is given by Lamb (1945, p. 85), and one obtains for the kinetic energy of the motion

$$T = -\tfrac{1}{2}\pi\rho b^2 U^2, \tag{A 1}$$

and for the potential of the flow at the surface of the lamina

$$\phi = \pm U(b^2 - y^2)^{\frac{1}{2}}, \tag{A 2}$$

where y is the co-ordinate in the plane of the lamina, measured from its centre. The impulse of the motion is given by

$$P = dT/dU = \pi\rho b^2 U, \tag{A 3}$$

and the surface velocity by

$$d\phi/dy = \pm Uy(b^2-y^2)^{-\frac{1}{2}}. \tag{A 4}$$

If the lamina were suddenly dissolved away, the flow could be considered as being produced by a distribution of rectilinear vortices over the surface of the lamina. These vortices tend to roll up to form a linear vortex pair with the centres of the cores located near the edges of the lamina where the vorticity is strongest. It is assumed that the vorticity is uniformly distributed over the cores. Let the distance between the centres of the cores be denoted by $2B$. The velocity of a vortex pair relative to the surrounding gas, and its impulse, are given by (Lamb 1945, pp. 221, 229)

$$v = K/4\pi B \tag{A 5}$$

and

$$P' = 2BK\rho, \tag{A 6}$$

respectively, where the circulation around the cores is $+K$ and $-K$. With the aid of equation (A 4), one obtains for the circulation

$$K = 2\int_0^b Uy(b^2-y^2)^{-\frac{1}{2}}\,dy = 2Ub. \tag{A 7}$$

Rolling up of the vortex elements does not affect the impulse of the motion, so that $P' = P$ and equations (A 3), (A 6) and (A 7) yield

$$B = \tfrac{1}{4}\pi b. \tag{A 8}$$

If this result is substituted into equation (A 5), one obtains

$$v = (2/\pi^2)\,U = 0{\cdot}203\,U. \tag{A 9}$$

In view of the hypothesis made for the motion of a gas bubble, U and v must be identified with the velocities of the initial and final bubble motion relative to the surrounding gas, so that $U = u_P - u_G$ and $v = u_B - u_G$. Equation (A 9) thus yields the final result $\beta = 0{\cdot}203$.

REFERENCES

Birkhoff, G. & Caywood, T. E. 1949 *Fluid flow patterns. J. Appl. Phys.* **20**, 646.

Bomelburg, H. J. 1956 A method for the measurement of the flow of air by means of series of electric sparks. *Univ. of Marland, Tech. Note* BN–68, AFOSR-TN-56-38.

Cady, W. M. 1954 In *Physical Measurements in Gas Dynamics and Combustion, High Speed Aerodynamics and Jet Propulsion*, pp. 139–58, vol. ix. Princeton: Princeton University Press.

Herzog, J. 1957 A new experimental approach to the analysis of compressor performance. *Univ. of Maryland, Tech. Note* BN-90, AFOSR-TN-57-3.

Herzog, J. & Weske, J. R. 1957 Characteristics of the technique of aerodynamic investigation by means of electric sparks. *Univ. of Maryland, Tech. Note* BN-105, AFOSR-57-359.

Hirschfelder, J. O., Curtis, C. F. & Bird, R. B. 1954 *Molecular Theory of Gases and Liquids*. New York: Wiley.

Hoenig, S. A. 1957 Acceleration of dust particles by shock waves. *J. Appl. Phys.* **28**, 1218.

Lamb, H. 1945 *Hydrodynamics*, 6th ed. New York: Dover.

Markstein, G. H. 1957 A shock tube study of flame front-pressure wave interaction. *6th Symposium (International) on Combustion*, pp. 387–98. New York: Reinhold.

Markstein, G. H. 1958 Discussion of Rudinger 1958.

RUDINGER, G. 1958 Shock wave and flame interactions. *Combustion and Propulsion*, pp. 153–82. Third AGARD Coll. London: Pergamon.

SAHEKI, Y. 1947 On the measurement of wind (tunnel) velocity (distributions) by the electric spark method. *Hokkaido Univ., Faculty of Engineering Memoirs*, **8**, 185; transl. by E. Hope, *Nat. Res. Counc. Can. Tech. Trans.* TT-100 (1950).

TAYLOR, G. I. 1953 Formation of a vortex ring by giving an impulse to a circular disk and then dissolving it away. *J. Appl. Phys.* **24**, 104.

TOWNEND, H. C. H. 1937 Visual and photographic methods of studying boundary layer flow. *Aero. Res. Counc. (Gt Brit.), Res. and Mem.* no. 1803.

TURNER, J. S. 1957 Buoyant vortex rings. *Proc. Roy. Soc.* A, **239**, 61.

WESKE, J. R. 1958 Ein Beitrag zur Untersuchung stetiger und unstetiger dreidimensionaler Strömungsfelder in Turbomaschinen. *ZAM* IXb (5/6) 721 (J. Ackeret Anniversary issue).

WRIGHT, F. H. 1951 The particle-track method of tracing fluid streamlines. *Jet Propulsion Lab., Calif. Inst. of Technology, Progress Rept*, no. 3–23.

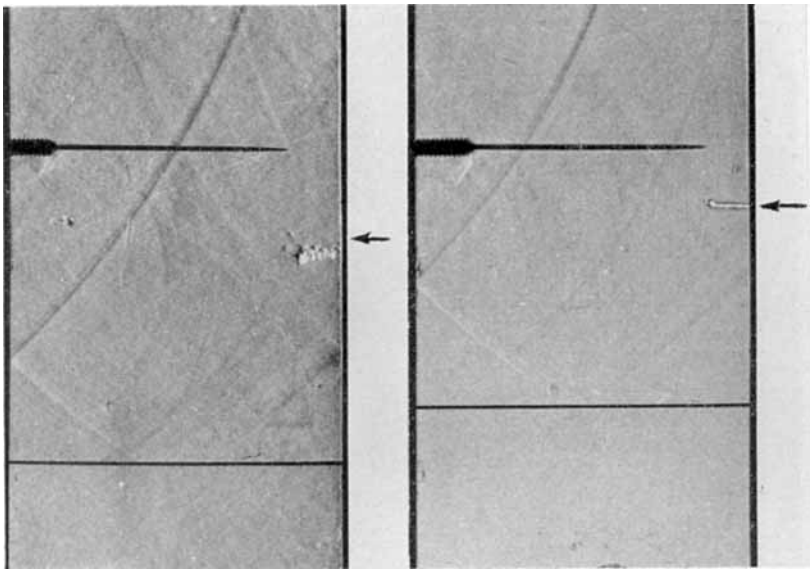

(*a*) (*b*)

FIGURE 2. Typical schlieren photographs of spark columns with the spark discharged (*a*) before, and (*b*) after, passage of a shock wave (pressure ratio 1·58). Arrows indicate calculated displacements of an unheated air element that initially was at the location of the spark gap.

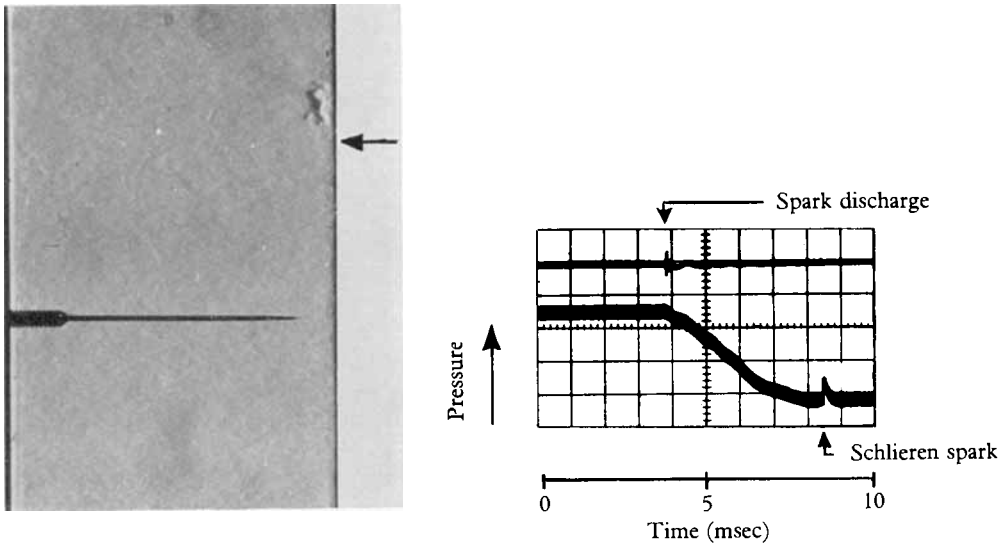

FIGURE 5. Schlieren photograph of spark bubble after acceleration by expansion wave and its reflexion from the closed bottom of the shock tube (overall pressure ratio 0·66). Pressure record is taken a few inches above spark gap. Arrow indicates calculated displacement of an unheated air element that initially was at the location of the spark gap.

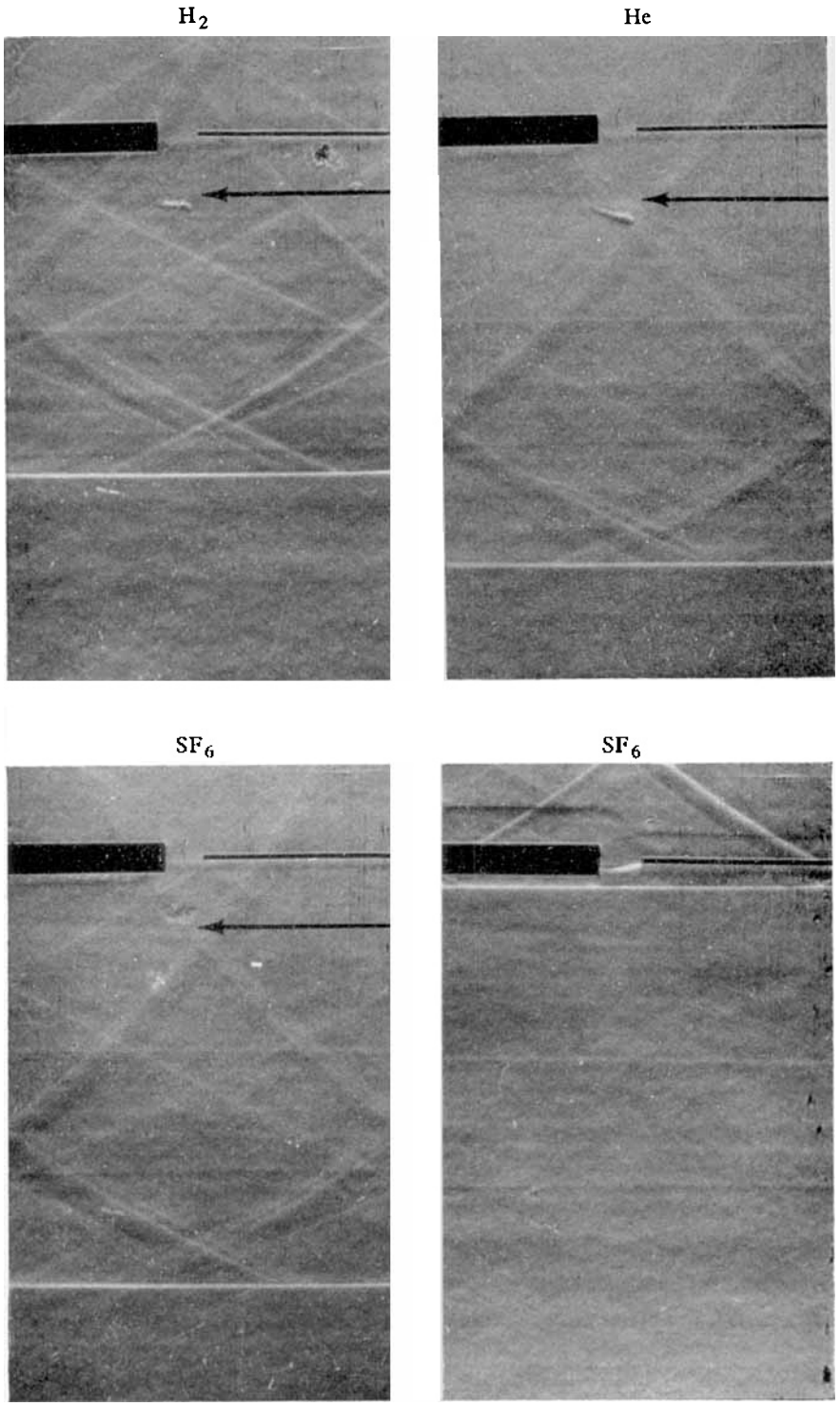

FIGURE 6. Typical gas jet/shock-wave interactions (shock pressure ratio 1·58).

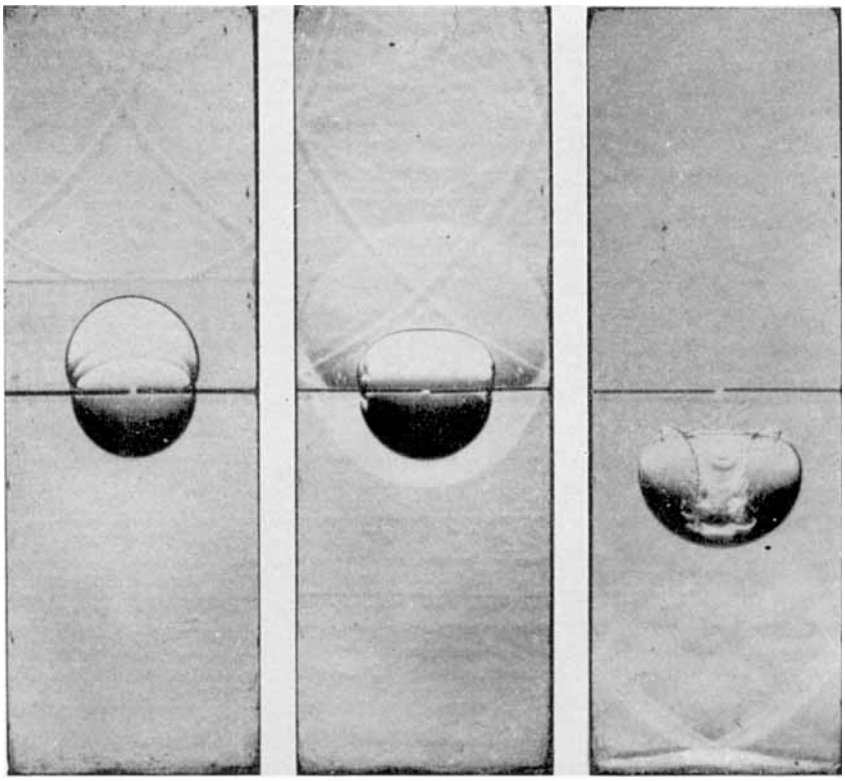

0·0 0·1 0·4

Milliseconds after interaction

FIGURE 7. Interaction of a shock wave (pressure ratio about 1·3) with a bubble of burned gas (stoichiometric butane–air mixture).